10. South, T. L., Blake, P. R., Hare, D. R. & Summers, M. F. C-terminal retroviral-type zinc finger domain from the HIV-1 nucleocapsid protein is structurally similar to the N-terminal zinc finger domain. *Biochemistry* **30,** 6342–6349 (1991).
11. Luisi, B. F. *et al*. Crystallographic analysis of the interaction of the glucorticoid receptor with DNA. *Nature* **352,** 497–505 (1991).
12. Marmorstein, R., Carey, M., Ptashne, M. & Harrison, S. C. DNA recognition by GAL4: structure of a protein–DNA complex. *Nature* **356,** 408–414 (1992).
13. Everett, R. D. *et al*. A novel arrangement of zinc-binding residues and secondary structure in the C3HC4 motif of an alpha herpes virus protein family. *J. Mol. Biol.* **234,** 1038–1047 (1993).
14. Barlow, P. N., Luisi, B., Milner, A., Elliot, M. & Everett, R. Structure of the C_3HC_4 domain by ^{1}H-nuclear magnetic resonance spectroscopy. *J. Mol. Biol.* **237,** 201–211 (1994).
15. Borden, K. L. B. *et al*. The solution structure of the RING finger domain from the acute promyelocytic leukaemia proto-oncoprotein PML. *EMBO J.* **14,** 1532–1541 (1995).
16. Phillips, S. E. V. The β-ribbon DNA recognition motif. *Ann. Rev. Biophys. Biomol. Struct.* **23,** 671–701 (1994).
17. Kim, J. L., Nikolov, D. B. & Burley, S. K. Co-crystal structure of TBP recognizing the minor groove of a TATA element. *Nature* **365,** 520–527 (1993).
18. Kim, Y., Geiger, J. H., Hahn, S. & Sigler, P. B. Crystal structure of a yeast TBP–TATA-box complex. *Nature* **365,** 512–520 (1993).
19. Schumacher, M. A., Choi, K. Y., Zalkin, H. & Brennan, R. G. Crystal structure of LacI member, PurR, bound to DNA: minor groove binding by α-helices. *Science* **266,** 763–770 (1994).
20. Flick, K. E. *et al*. Crystallization and preliminary X-ray studies of I-PpoI: a nuclear, intron-encoded homing endonuclease from *Physarum polycephalum*. *Protein Sci.* **6,** 1–4 (1997).
21. Otwinowski, Z. & Minor, W. Processing of X-ray diffraction data collected in oscillation mode. *Methods Enzymol.* **276,** 307–326 (1997).
22. Leslie, A. G. W. in *Joint CCP4 and ESF-EACMB Newsletter on Protein Crystallography* (Daresbury Laboratory, Warrington, UK, 1992).
23. CCP4 *The SERC (UK) Collaborative Computing Project No. 4, a Suite of Programs for Protein Crystallography* (Daresbury Laboratory, Warrington, UK, 1979).
24. QUANTA96 *X-ray Structure Analysis User's Reference* (Molecular Simulations, San Diego, 1996).
25. Brünger, A. *XPLOR version 3.1: A System for X-ray Crystallography and NMR* (Yale Univ. Press, New Haven, CT, 1992).
26. Laskowski, R. J., Macarthur, M. W., Moss, D. S. & Thornton, J. M. PROCHECK: a program to check the stereochemical quality of protein structures. *J. Appl. Crystallogr.* **26,** 383–290 (1993).
27. Evans, S. V. SETOR: hardware-lighted three-dimensional solid model representations of macromolecules. *J. Mol. Graphics* **11,** 134–138 (1993).

Acknowledgements. We thank D. McHugh, K. Stephens and J. D. Heath for initial subcloning, purification and crystallization studies; R. Strong, K. Zhang and B. Scott for advice during the crystallographic analysis; and the beamline staff at the Advanced Light Source (NLBL laboratories), beamline 5.0.2, particularly T. Earnest, for assistance. B.L.S. and R.J.M. are funded for this project by the NIH. K.E.F. was supported by an NIH training grant and the American Heart Associaiton. M.S.J. was supported by an NSF fellowship and an NIH training grant.

Correspondence and requests for materials and coordinates should be addressed to B.L.S. (e-mail: bstoddar@fred.fhcrc.org). Coordinates have been deposited in the Brookhaven Protein Data Bank (accession nos lipp, 1a73, 1a74).

corrections

Emergence of symbiosis in peptide self-replication through a hypercyclic network

David H. Lee, Kay Severin, Yohei Yokobayashi & M. Reza Ghadiri

Nature **390,** 591–594 (1997)

Hypercycles are based on second-order (or higher) autocatalysis and defined by two or more replicators that are connected by another superimposed autocatalytic cycle. Our study describes a mutualistic relationship between two replicators, each catalysing the formation of the other, that are linked by a superimposed catalytic cycle. Although the kinetic data suggest the intermediary of higher-order species in the autocatalytic processes, the present system should not be referred to as an example of a minimal hypercycle in the absence of direct experimental evidence for the autocatalytic cross-coupling between replicators. □

The complete genome sequence of the hyperthermophilic, sulphate-reducing archaeon *Archaeoglobus fulgidus*

Hans-Peter Klenk, Rebecca A. Clayton, Jean-Francois Tomb, Owen White, Karen E. Nelson, Karen A. Ketchum, Robert J. Dodson, Michelle Gwinn, Erin K. Hickey, Jeremy D. Peterson, Delwood L. Richardson, Anthony R. Kerlavage, David E. Graham, Nikos C. Kyrpides, Robert D. Fleischmann, John Quackenbush, Norman H. Lee, Granger G. Sutton, Steven Gill, Ewen F. Kirkness, Brian A. Dougherty, Keith McKenney, Mark D. Adams, Brendan Loftus, Scott Peterson, Claudia I. Reich, Leslie K. McNeil, Jonathan H. Badger, Anna Glodek, Lixin Zhou, Ross Overbeek, Jeannine D. Gocayne, Janice F. Weidman, Lisa McDonald, Teresa Utterback, Matthew D. Cotton, Tracy Spriggs, Patricia Artiach, Brian P. Kaine, Sean M. Sykes, Paul W. Sadow, Kurt P. D'Andrea, Cheryl Bowman, Claire Fujii, Stacey A. Garland, Tanya M. Mason, Gary J. Olsen, Claire M. Fraser, Hamilton O. Smith, Carl R. Woese & J. Craig Venter

Nature **390,** 364–370 (1997)

The pathway for sulphate reduction is incorrect as published: in Fig. 3 on page 367, adenylyl sulphate 3-phosphotransferase (*cysC*) is not needed in the pathway as outlined, as adenylyl sulphate reductase (*aprAB*) catalyses the first step in the reduction of adenylyl sulphate. The correct sequence of reactions is: sulphate is first activated to adenylyl sulphate, then reduced to sulphite and subsequently to sulphide. The enzymes catalysing these reactions are: sulphate adenylyltransferase (*sat*), adenylylsulphate reductase (*aprAB*), and sulphite reductase (*dsrABD*). We thank Jens-Dirk Schwenn for bringing this error to our attention. □

(that is, on its left side in Fig. 2a and b), a 231-nm-thick $Al_{0.165}Ga_{0.835}As$ spacer layer was grown with two Si δ-doping layers ($1 \times 10^{12}\,cm^{-2}$), one inserted 22 nm and the other 187 nm from the left edge of the deep well. A 10-nm-thick undoped GaAs region capped the structure. The spacer layer thickness was adjusted to preserve the same distance between the δ-doping layers and the double-quantum-well system, and therefore the electrostatic potentials are identical in both structures. The δ-doping provides a two-dimensional electron gas in the deep well with a calculated sheet electron density of $n_s = 4 \times 10^{11}\,cm^{-2}$.

For the absorption measurements, we processed our samples in a multipass (six) 45° wedge waveguide. This geometry allowed us to couple in linearly polarized radiation with a large component of the polarization normal to the layer (50%) as required by the intersub-band absorption selection rule[9]. The absorption was measured with a Fourier-transform infrared spectrometer (FTIR) using a step-scan modulation technique[10] in which the electron gas in the double well is periodically depopulated by a Ti/Au Shottky barrier contact evaporated on the surface of the sample and the two-dimensional electron gas is contacted by indium balls alloyed into the layer.

The absorption measurements at $T = 10\,K$ for both structures are compared in Fig. 3 with the results of numerical calculations using the coupled Schrödinger's and Poisson's equations. As predicted, the absorption strength at photon energies between the two resonances is strongly suppressed or enhanced by the interference effect depending on the location of the thin barrier, proving that tunnelling through the latter controls the interference effect when the broadening of the states is dominated by tunnelling. However, the finite broadening introduced by interface disorder prevents full quantum interference; this is the main reason for the departure from the calculated profiles and specifically the reason why the absorption does not vanish in the sample with destructive interference. Indeed, linewidth measurements on samples with the same coupled-well structure but with negligible tunnelling to the continuum showed a full-width at half-maximum of the absorption peaks of $\Gamma = 5\,meV$. This structure consists of an identical double quantum well between two 60-nm-thick $Al_{0.33}Ga_{0.67}As$ barriers. This value is a measure of the non-tunnelling contribution to the broadening of the optical transitions; it is smaller but not negligible compared with the calculated broadening by tunnelling through the 1.5 nm barrier, $\Gamma_1 \cong \Gamma_2 \cong 16\,meV$.

Destructive interference in intersub-band absorption in a double-well structure coupled by tunnelling to a continuum has recently been inferred from a fit of the absorption lineshape to a model that included the collision broadening in a phenomenological manner[11]. The present experiment gives more direct evidence of tunnelling-induced quantum interference by showing that tunnelling can be used to control the sign of the interference.

It is important to stress the difference between the phenomena described here and the Fano interference in intersub-band absorption recently reported by us[12]. In that work a minimum in the absorption arises because of interference between matrix elements for the ground state to the continuum and to a single resonance coupled by tunnelling to the same continuum. This leads to a strongly asymmetric absorption lineshape. In contrast, in the phenomena studied here interference arises between absorption paths through two resonances coupled to a continuum, and the direct matrix element from the ground state to the continuum is negligible.

These findings are relevant for the design of semiconductor lasers without population inversion (LWI). Such lasing action has so far been observed only in gases[4,5]. Essential for LWI is nonreciprocity between emission and absorption. A possible semiconductor LWI scheme would use the quantum-well structure of Fig. 2a for the active regions. The latter would be alternated with electron injectors as in quantum cascade lasers[13]. Electrons would be injected from the thick barrier side at an energy between the two resonances where the absorption cross-section is a minimum, to ensure strong non-reciprocity between intersub-band absorption and emission[7,8]. Although the realization of such a laser would be scientifically important, its implementation would be difficult and its technological impact limited by the very short lifetime (a few tenths of picoseconds) of the excited state which is required to achieve strong interference[14]. □

Received 23 June; accepted 6 October 1997.

1. Fano, U. Effect of configuration interaction on intensity and phase shifts. *Phys. Rev.* **124,** 1866–1878 (1961).
2. Harris, S. E. Lasers without inversion: interference of lifetime-broadened resonance. *Phys. Rev. Lett.* **62,** 1033–1035 (1989).
3. Arkhipkin, V. G. & Heller, Y. I. Radiation amplification without population at transitions to autoionizing states. *Phys. Lett. A* **98,** 12–14 (1983).
4. Zibrov, S. *et al.* Experimental demonstration of laser without population inversion via quantum interference in Rb. *Phys. Rev. Lett.* **75,** 1499–1452 (1995).
5. Padmadandu, G. G. *et al.* Laser oscillation without population inversion in a Sodium atomic beam. *Phys. Rev. Lett.* **76,** 2053–2056 (1996).
6. Boller, K.-J., Imamoglu, A. & Harris, S. E. Observation of electromagnetically induced transparency. *Phys. Rev. Lett.* **66,** 2593–2596 (1991).
7. Imamoglu, A. & Harris, S. E. Lasers without inversion: interference of dressed lifetime-broadened states. *Opt. Lett.* **13,** 1344–1346 (1989).
8. Imamoglu, A & Ram, R. J. Semiconductor lasers without population inversion. *Opt. Lett.* **19,** 1744–1746 (1994).
9. Levine, B. F., Choi, K. K., Bethea, C. G., Walker, J. & Malik, R. J. New 10 μm infrared detector using intersubband absorption in resonant tunneling GaA1As superlattices. *Appl. Phys. Lett.* **50,** 1092–1094 (1987).
10. Faist, J. *et al.* Narrowing of the intersubband electroluminescence spectrum in coupled-quantum-well heterostructures. *Appl. Phys. Lett.* **65,** 94–96 (1994).
11. Smidt, H., Campman, K. L., Gossard, A. C. & Imamoglu, A. Tunnel induced transparency: Fano interference in intersubband transitions. *Appl. Phys. Lett.* **70,** 3455–3457 (1997).
12. Faist, J. *et al.* Tunable Fano interference in intersubband absorption. *Opt. Lett.* **21,** 985–987 (1996).
13. Capasso, F., Faist, J., Sirtori, C. & Cho, A. Y. Infrared (4–11 μm) quantum cascade lasers. *Solid State Commun.* **102,** 231–236 (1997).
14. Kurghin, J. B. & Rosencher, E. Practical aspects of lasing without inversion in various media. *IEEE J. Quant. Electron.* **QE-32,** 1882–1890 (1996).

Acknowledgements. We thank S. Harris, A. Imamoglu, R. J. Ram, A. Tredicucci and C. Gmachl for enlightening discussions, and the authors of ref. 11 for making their manuscript available before publication. The work was supported in part by DARPA/ARO.

Correspndence should be addressed to F.C. (e-mail: fc@bell-labs.com or fc@lucent.com).

Emergence of symbiosis in peptide self-replication through a hypercyclic network

David H. Lee, Kay Severin, Yohei Yokobayashi & M. Reza Ghadiri

Departments of Chemistry and Molecular Biology, and the Skaggs Institute for Chemical Biology, The Scripps Research Institute, La Jolla, California 92037, USA

Symbiosis is an association between different organisms that leads to a reciprocal enhancement of their ability to survive. Similar mutually beneficial relationships can operate at the molecular level in the form of a hypercycle, a collective of two or more self-replicating species interlinked through a cyclic catalytic network[1–5]. The superposition of cross-catalysis onto autocatalytic replication integrates the members of the hypercycle into a single system that reproduces through a second-order (or higher) form of nonlinear autocatalysis. The hypercycle population as a whole is therefore able to compete more efficiently for existing resources than any one member on its own. In addition, the effects of beneficial mutations of any one member are spread over the entire population. The formation of hypercycles has been suggested as an important step in the transition from inanimate to living chemistry[6] , and a large number of hypercycles are expected to be embedded within the complex networks of living systems[7]. But only one naturally occurring hypercycle has been well documented[8], while two autocatalytic chemical systems may contain vestiges of hypercyclic organization[9,10]. Here we report a

chemical system that constitutes a clear example of a minimal hypercyclic network, in which two otherwise competitive self-replicating peptides symbiotically catalyse each others' production.

The present design of a minimal hypercycle is based on two self-replicating coiled coil peptides $\mathbf{R_1}$ and $\mathbf{R_2}$ (Fig. 1). The replicator $\mathbf{R_1}$ was recently reported[11,12] and is produced as the ligation product of the electrophilic peptide fragment **E** and the nucleophilic fragment $\mathbf{N_1}$. The replicator $\mathbf{R_2}$ is made from the same electrophilic fragment but a different nucleophilic peptide fragment $\mathbf{N_2}$. The nucleophilic fragments $\mathbf{N_1}$ and $\mathbf{N_2}$ differ in their sequence at the hydrophobic recognition surface—$\mathbf{N_1}$ is composed of valine and leucine whereas $\mathbf{N_2}$ is made up of isoleucine and leucine residues. This difference in sequence at the hydrophobic core is known to affect profoundly the aggregation state of coiled coils[13,14]. Furthermore it is known that conservative mutations in this region of the structure can drastically alter the kinetic behaviour of the replicator[11,12,15].

The ability of $\mathbf{R_2}$ to self-replicate was determined by observation of characteristics previously established as signatures of self-replication (Fig. 2)[11,12]. Similar to that of $\mathbf{R_1}$, the new replicator $\mathbf{R_2}$ also displays a parabolic growth profile. Numerical fitting of the kinetic data obtained for $\mathbf{R_2}$ to the empirical rate equations of von Kiedrowski[16] gave a background rate constant $k_b = 0.072 \pm 0.005\,M^{-1}\,s^{-1}$ and an apparent autocatalytic rate constant $k_a = 52 \pm 1\,M^{-3/2}\,s^{-1}$, making $\mathbf{R_2}$ more efficient than its relative $\mathbf{R_1}$ ($k_b = 0.063\,M^{-1}\,s^{-1}$ and constant $k_a = 29.4\,M^{-3/2}\,s^{-1}$).

A solution containing all three fragments **E**, $\mathbf{N_1}$ and $\mathbf{N_2}$ gave a combinatorial synthesis of both replicators. *A priori*, one would expect a survival-of-the-fittest situation where the more efficient replicator $\mathbf{R_2}$ would overwhelm $\mathbf{R_1}$ by consuming the common fragment **E** more quickly. At first glance, this expectation seemed to be borne out as $\mathbf{R_2}$ was produced in greater abundance than $\mathbf{R_1}$ (as expected, when molecular interactions are disrupted in the presence of guanidinium hydrochloride, no kinetic preference for $\mathbf{R_2}$ over $\mathbf{R_1}$ was observed). However, the situation is more interesting and complex. When we sought to give $\mathbf{R_1}$ an advantage in this competition by adding 40% $\mathbf{R_1}$ (with respect to the nucleophile concentration) at the start of the reaction, to our surprise the rate of $\mathbf{R_1}$ self-production increased by only 1.7 times over the unseeded reaction but the rate of $\mathbf{R_2}$ formation was enhanced to a greater extent, by 5.4 times (Table 1, Fig. 3). Thus the two replicators are not mutually exclusive in their growth; $\mathbf{R_1}$ catalyses the formation of $\mathbf{R_2}$ as well as itself. Likewise, perturbation of the reaction by seeding it with 45% $\mathbf{R_2}$ not only increased the rate of $\mathbf{R_2}$ production 2.9 times but $\mathbf{R_1}$ as well, by 3.5 times. Thus a cross-catalytic cycle is cooperatively coupled with two self-replicating reactions, making this system one which is hypercyclic in nature. There are four characteristic outcomes expected for such a hypercyclic network, depending on the relative efficiencies of the coupled catalytic and autocatalytic reactions[2]. The observed greater efficiencies of the catalytic reactions over the autocatalytic components of the system are the most desirable outcomes which assure the stability of the hypercycle: production of one species promotes the production of the other to an even greater degree. This particular mode of catalytic coupling prevents one replicator from overwhelming the other and enables the two to reproduce as a single coherent unit.

To verify that $\mathbf{R_1}$ and $\mathbf{R_2}$ catalyse each other's production, the

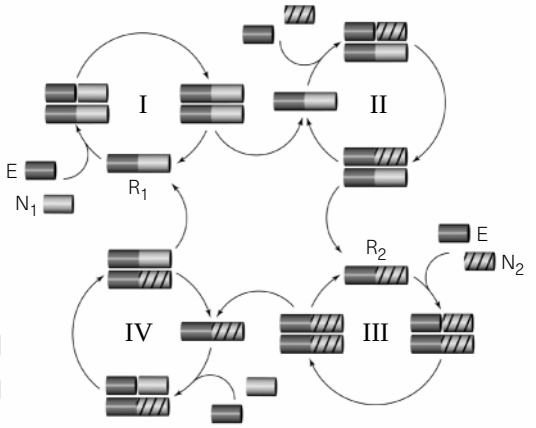

Figure 1 Schematic diagram of a minimal hypercycle based on two self-replicating peptides. Cycles I and III show the self-producing cycles of replicators $\mathbf{R_1}$ (dark grey/light grey) and $\mathbf{R_2}$ (dark grey/striped) respectively, which pre-organize their constituent fragments thereby promoting peptide ligation. Cycle II, where $\mathbf{R_1}$ promotes $\mathbf{R_2}$ formation, and cycle IV, where $\mathbf{R_2}$ promotes $\mathbf{R_1}$ formation, comprise the catalytic components of the hypercycle and allow the replicators to positively regulate each others' production. The mechanistic details of the present hypercyclic network may be more complex than the minimal system depicted here. Detailed kinetic analyses of the replicator sequences have shown that the autocatalytically productive intermediates involve, at least in part, quaternary complexes in which two template strands pre-organize the reactive peptide fragments (ref. 12 and K. Kumar, D.H.L., M.R.G., unpublished results). The following peptide sequences were employed in this study: replicator 1 ($\mathbf{R_1}$), ArCONH-RMKQLEEKVYELLSKVA-CLEXEVARLKKLVGE-$CONH_2$; replicator 2 ($\mathbf{R_2}$), ArCONH-RMKQLEEKVYELLSKVA-CLEXEIARLKKLIGE-$CONH_2$; electrophilic fragment (**E**), ArCONH-RMKQLEEKVYELLSKVA-COSBn; nucleophilic fragment 1 ($\mathbf{N_1}$), H_2N-CLEXEVARLKKLVGE-$CONH_2$; nucleophilic fragment 2 ($\mathbf{N_2}$), H_2N-CLEXEIARLKKLIGE-$CONH_2$. Bn, benzyl; Ar, 4-acetamidophenyl; and X, lysine-ε-NHCO-Ar.

Table 1 Initial rates of product formation

Product	No replicators added	+40% $\mathbf{R_1}$	+45% $\mathbf{R_2}$
$\mathbf{R_1}$	4.8	8.2	17.0
$\mathbf{R_2}$	5.8	31.1	16.9

The data in this table (in units of $10^{-8}\,M\,min^{-1}$) are for reactions containing the three peptide fragments in the absence and presence of added replicators.

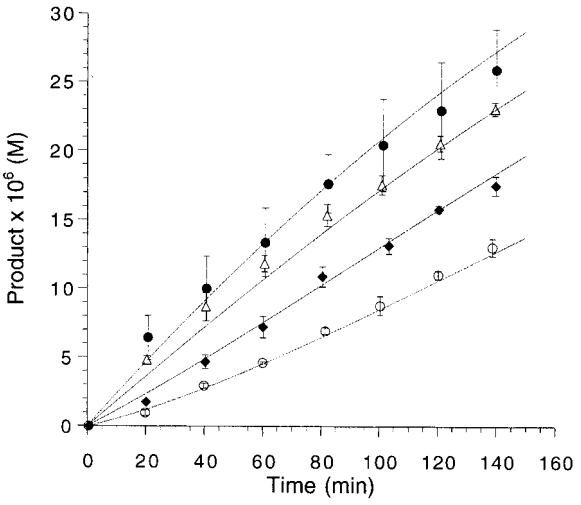

Figure 2 Production of $\mathbf{R_2}$ as a function of time in the presence of various initial concentrations of $\mathbf{R_2}$. Open circles, in the absence of any added $\mathbf{R_2}$; filled diamonds, in the presence of 4.0 μM; open triangles, in the presence of 21.4 μM; and filled circles, 42.6 μM of initially added $\mathbf{R_2}$. Curves were generated by nonlinear least-squares fit of the data to the empirical rate equation of von Kiedrowski using the program SimFit[16]. Data are an average of two experiments.

reaction mixtures were simplified to include **E** and only one nucleophile, and then seeded with the template that was not produced *in situ* (Fig. 4). Comparisons with unseeded reactions revealed that even in these simplified systems one template can promote the formation of the other, giving rate enhancements much larger than what would be expected if the reaction mixture were seeded with the autocatalytic template. Reaction mixtures containing **E** and $\mathbf{N_1}$ that were seeded with 25% $\mathbf{R_2}$ enhanced the initial rate of production of $\mathbf{R_1}$ from $3.9 \times 10^{-8}\,\mathrm{M\,min^{-1}}$ to $1.5 \times 10^{-7}\,\mathrm{M\,min^{-1}}$, a 3.8 times increase over the unseeded reaction. Seeding of the same reaction mixture with 25% $\mathbf{R_1}$ would improve the rate by only 2.8 times. Similarly, seeding reaction mixtures containing **E** and $\mathbf{N_2}$ with 35% $\mathbf{R_1}$ gave a 5.4 times rate enhancement over the $5.0 \times 10^{-8}\,\mathrm{M\,min^{-1}}$ rate observed for the reaction without added catalyst. The increase is greater than the 3.6 times enhancement expected for the autocatalytic reaction containing 35% $\mathbf{R_2}$.

We now consider the sequence selectivity issues in the formation of the hypercyclic peptide network. The operation of the hypercycle is based on complementary, as well as self-complementary, forms of catalysis. As noted below, there is mounting evidence that both processes are strongly sequence selective. Previously we had shown that in the case of replicator $\mathbf{R_1}$, even conservative mutations (Val9Ala—where a valine has been substituted by an alanine at position 9—and Leu26Ala) in the hydrophobic core residues completely abolish the autocatalytic process[11–12]. In this study we have determined that similar replicator $\mathbf{R_2}$ mutations are also autocatalytically infertile. There is also good evidence for high sequence selectivity in the cross-catalytic component of the system. Control studies have indicated that the Leu26Ala $\mathbf{R_2}$ mutant cannot cross-catalyse the formation of replicators $\mathbf{R_1}$ nor $\mathbf{R_2}$. Although in a recent study[15] we have shown that the Val9Ala $\mathbf{R_1}$ mutant can efficiently cross-catalyse the formation of $\mathbf{R_1}$, we have found it to be ineffective in catalysing $\mathbf{R_2}$ production. Moreover, in a related study we have shown that diminution in the initial rate of peptide fragment condensation of more than 3 orders of magnitude can be caused even by electrostatic substitutions at the solvent-exposed *e* and *g* positions of the heptad repeat sequence[17]. Although the above studies strongly support high sequence selectivity in the catalytic and autocatalytic components of the hypercyclic network, a significantly large sequence-space must undoubtedly exist that would enable the spontaneous self-organization of even more complex networks. Studies along those lines are under investigation.

The work reported here may have particular relevance to various origin-of-life theories[1–4,18]. It has been suggested that at the dawn of life the onset of darwinian evolution must have been marked by

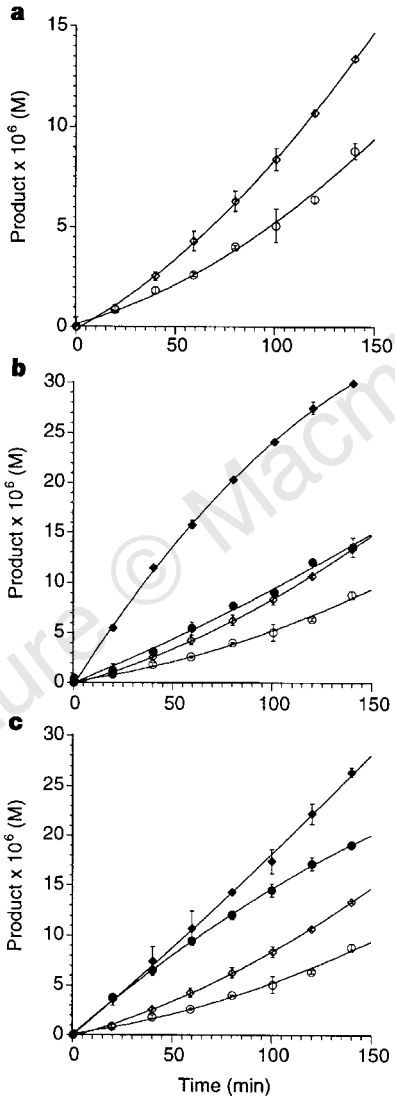

Figure 3 Replicators $\mathbf{R_1}$ and $\mathbf{R_2}$ self-organize into a two-membered hypercyclic network. **a**, Production of $\mathbf{R_1}$ (empty circles) and $\mathbf{R_2}$ (empty diamonds) as a function of time for reaction mixtures containing **E**, $\mathbf{N_1}$ and $\mathbf{N_2}$. **b**, Formation of $\mathbf{R_1}$ (filled circles) and $\mathbf{R_2}$ (filled diamonds) as a function of time for reaction mixtures containing the three fragments and 40% $\mathbf{R_1}$. **c**, Formation of $\mathbf{R_1}$ (filled circles) and $\mathbf{R_2}$ (filled diamonds) as a function of time for reaction mixtures containing the three fragments and 45% $\mathbf{R_2}$. In **b** and **c**, production formation in the absence of added templates are shown for comparison. Data are an average of two experiments. Curves are shown to guide the eye.

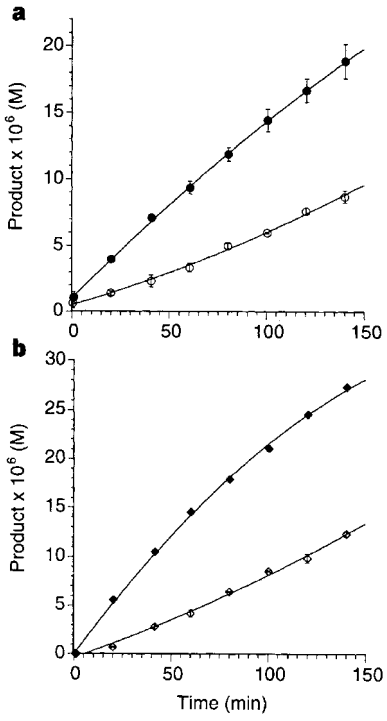

Figure 4 Replicators $\mathbf{R_1}$ and $\mathbf{R_2}$ are cross-catalytic. **a**, Formation of $\mathbf{R_1}$ as a function of time for the reaction mixture containing only **E** and $\mathbf{N_1}$ in the absence (empty circles) and in the presence (filled circles) of 35% $\mathbf{R_2}$. **b**, Formation of $\mathbf{R_2}$ as a function of time for the reaction mixture containing **E** and $\mathbf{N_2}$ in the absence (empty diamonds) and in the presence (filled diamonds) of 25% $\mathbf{R_1}$. Data are an average of two experiments. Curves are shown to guide the eye.

selection based on feedback processes of genotype replication[19]. It is also likely that molecular genotypes and phenotypes may have been the very same molecules[20]. Our example of a hypercyclic peptide network supports the idea that peptides could play a role in both hypotheses. □

Methods

Self-replication of R_2. All reactions were done in 0.6 ml Eppendorf tubes at 23 °C. A stock solution containing **E**, $\mathbf{N_2}$ and the internal standard 4-acetamidobenzoic acid (ABA), were seeded with various amounts of $\mathbf{R_2}$. Benzylmercaptan (1 μl) was then added. Reactions were initiated by adding 3-(N-morpholino)propanesulphonic acid (MOPS) buffer (pH = 7.50, 200 mM, 236 μl), giving a total volume of 300 μl and concentrations of $[\mathbf{N_2}] = 104.5\,\mu M$, $[\mathbf{E}] = 94.2\,\mu M$, $[\mathbf{R_2}] = 0$. 4.0, 21.4 or 42.6 μM. [MOPS] = 157 mM, [ABA] = 40.4 μM. Samples (30 μl) were taken at various time points and quenched with 2% trifluoroacetic acid (TFA) in water (70 μl) then stored at −70 °C. Samples were analysed by high pressure liquid chromatography on a Zorbax C8 column using an acetonitrile/water/0.1% TFA gradient while monitoring at 270 nm. The identity of all peptides was determined by mass spectrometry and verified by coinjection with authentic samples. Experiments were done in duplicate.

Determination of hypercyclic organization in the $E/N_1/N_2$ mixture. Reactions were done as described above except that the stock solution contained, besides **E** and ABA, both $\mathbf{N_1}$ and $\mathbf{N_2}$, which was subsequently seeded with either $\mathbf{R_1}$, $\mathbf{R_2}$, or water. Reactions were initiated by adding MOPS buffer (pH = 7.50, 200 mM, 236.6 μl), giving a total volume of 300 μl and concentrations of $[\mathbf{N_1}] = 112.5\,\mu M$, $[\mathbf{N_2}] = 112.7\,\mu M$, $[\mathbf{E}] = 91.1\,\mu M$, [MOPS] = 157.7 mM, $[ABA] = 97.1\,\mu M$, $[\mathbf{R_1}] = 45.1\,\mu M$, $[\mathbf{R_2}] = 50.4\,\mu M$.

Verification of the catalytic components of the hypercycle. Reactions were performed as described above except only one nucleophile was present in the reaction mixture and the reaction was seeded with the replicator that was not produced *in situ*. Initial concentrations are (1) $[\mathbf{E}] = 88.9\,\mu M$, $[\mathbf{N_1}] = 98.2\,\mu M$, $[\mathbf{R_2}] = 25.2\,\mu M$, $[ABA] = 50.5\,\mu M$; (2) $[\mathbf{E}] = 80.4\,\mu M$, $[\mathbf{N_{21}}] = 96.9\,\mu M$, $[\mathbf{R_1}] = 35.3\,\mu M$, $[ABA] = 36.9\,\mu M$.

Received 20 June; accepted 20 October 1997.

1. Eigen, M. & Schuster, P. The hypercycle. A principle of natural self-organization. Part A: emergence of the hypercycle. *Naturwissenschaften* **64,** 541–565 (1977).
2. Eigen, M. & Schuster, P. The hypercycle. A principle of natural self-organization. Part B: the abstract hypercycle. *Naturwissenschaften* **65,** 7–41 (1978).
3. Eigen, M. & Schuster, P. The hypercycle. A principle of natural self-organization. Part C: The realistic hypercycle. *Naturwissenschaften* **65,** 341–369 (1978).
4. Eigen, M. Self-organization of matter and the evolution of biological macromolecules. *Naturwissenschaften* **58,** 465–523 (1971).
5. Müller-Herold, U. What is a hypercycle? *J. Theor. Biol.* **102,** 569–584 (1983).
6. Lee, D. H., Severin, K. & Ghadiri, M. R. Autocatalytic networks: the transition from molecular self-replication to molecular ecosystems. *Curr. Opin. Chem. Biol.* (in the press).
7. Ricard, J. & Noat, G. Electrostatic effects and the dynamics of enzyme reactions at the surface of plant cells. 1. A theory of the ionic control of a complex multi-enzyme system. *Eur. J. Biochem.* **155,** 183–190 (1986).
8. Eigen, M., Biebricher, C. K., Gebinoga, M. & Gardiner, W. C. The hypercycle. Coupling of RNA and protein biosynthesis in the infection cycle of an RNA bacteriophage. *Biochemistry* **30,** 11005–11018 (1991).
9. Hong, J.-I., Feng, Q., Rotello, V. & Rebek, J. Jr Competition, cooperation and mutation: improving a synthetic replicator by light irradiation. *Science* **255,** 848–850 (1992).
10. Achilles, T. & von Kiedrowski, G. A self-replicating system from three starting materials. *Angew. Chem. Int. Edn Engl.* **32,** 1198–1201 (1993).
11. Lee, D. H., Granja, J. R., Martinez, J. A., Severin, K. S. & Ghadiri, M. R. A self-replicating peptide. *Nature* **382,** 525–528 (1996).
12. Severin, K. S., Lee, D. H., Martinez, J. A. & Ghadiri, M. R. Peptide self-replication via template-directed ligation. *Chem. Eur. J.* **3,** 1017–1024 (1997).
13. Harbury, P. B., Zhang, T., Kim, P. S. & Alber, T. A switch between two-, three- and four-stranded coiled coils in GCN4 leucine zipper mutants. *Science* **262,** 1401–1407 (1993).
14. Hu, J. C., O'Shea, E. K., Kim, P. S. & Sauer, R. T. Sequence requirements for coiled coils: analysis with λ repressor-GCN4 leucine zipper fusions. *Science* **250,** 1400–1403 (1990).
15. Severin, K., Lee, D. H., Martinez, J. A. & Ghadiri, M. R. Dynamic error-correction in an autocatalytic peptide network. *Angew. Chem. Int. Edn Engl.* (in the press).
16. von Kiedrowski, G. Minimal replicator theory I: parabolic versus exponential growth. *Bioorg. Chem. Front.* **3,** 113–146 (1993).
17. Severin, K., Lee, D. H., Kennan, A. J. & Ghadiri, M. R. A synthetic peptide ligase. *Nature* **389,** 706–709 (1997).
18. Kauffman, S. A. *The Origins of Order* (Oxford Univ. Press, New York, 1993).
19. Küppers, B.-O. *The Origin of Biological Information* (MIT Press, Cambridge, MA, 1990).
20. Joyce, G. F. RNA evolution and the origins of life. *Nature* **338,** 217–224 (1989).

Acknowledgements. We thank K. Kumar for discussions. We also thank the Medical Research Council of Canada for a predoctoral fellowship (D.H.L.), and the Deutsche Forschungsgemeinschaft for a postdoctoral fellowship (K.S.).

Correspondence and requests for materials should be addressed to M.R.G. (e-mail: ghadiri@scripps.edu).

Kinetic limitations on droplet formation in clouds

P. Y. Chuang*, R. J. Charlson† & J. H. Seinfeld‡

* *Department of Environmental Engineering Science, MC 138-78, California Institute of Technology, Pasadena, California 91125, USA*
† *Departments of Atmospheric Sciences and Chemistry, University of Washington, Seattle, Washington 98195, USA*
‡ *Division of Engineering and Applied Science and Department of Chemical Engineering, MC 210-41, California Institute of Technology, Pasadena, California 91125, USA*

The 'indirect' radiative cooling of climate due to the role of anthropogenic aerosols in cloud droplet formation processes (which affect cloud albedo) is potentially large, up to $-1.5\,W\,m^{-2}$ (ref. 1). It is important to be able to determine the number concentration of cloud droplets to within a few per cent, as radiative forcing as a result of clouds is very sensitive to changes in this quantity[2], but empirical approaches are problematic[3–5]. The initial growth of a subset of particles known as cloud condensation nuclei and their subsequent 'activation' to form droplets are generally calculated with the assumption that cloud droplet activation occurs as an equilibrium process described by classical Köhler theory[6,7]. Here we show that this assumption can be invalid under certain realistic conditions. We conclude that the poor empirical correlation between cloud droplet and cloud condensation nuclei concentrations is partly a result of kinetically limited growth before droplet activation occurs. Ignoring these considerations in calculations of total cloud radiative forcing based on cloud condensation nuclei concentrations could lead to errors that are of the same order of magnitude as the total anthropogenic greenhouse-gas radiative forcing[1].

Cloud droplet activation and subsequent treatments of cloud droplet growth in atmospheric models generally rely on the assumption that pre-activation growth is accurately described by an equilibrium model in which the particle diameter is always at equilibrium with the local supersaturation[6,7]. The equilibrium relationship between supersaturation and particle size for a particle composed of highly soluble inorganic species can be described by the well-known Köhler equation (curve A, Fig. 1)[8]. Cloud droplet nuclei (CDN) activate when they grow larger than their critical diameter, D_{pc}, after which they can grow spontaneously, limited only by growth kinetics. The concept of CDN is distinct from that of CCN in that, whereas CCN are defined as those particles that activate to become cloud droplets within a cloud chamber of fixed or prescribed supersaturation, CDN are those particles that actually activate in the atmosphere under conditions of time-varying supersaturation.

To evaluate the conditions under which the equilibrium activation model is valid, two timescales will be defined. One is the timescale for particle growth that would be required for that particle to remain at equilibrium as the ambient supersaturation ratio increases in a rising air parcel, τ_e. The other is the timescale for actual change in the droplet size resulting from condensational growth, τ_g. Hence, if $\tau_e \gg \tau_g$ then the equilibrium model is reasonable; otherwise, CDN activation, and hence the cloud droplet size distribution, can be accurately predicted only if the kinetics of droplet growth are considered. To calculate τ_e, the rate of change of the droplet diameter that would be required for that droplet to remain at its equilibrium size, dD_{pe}/dt, is determined from the combination of two effects. First, the time rate of change of supersaturation, dS/dt, can be determined using a simple one-dimensional adiabatic parcel model[9]. Next, the rate of change of D_{pe} with respect to supersaturation, dD_{pe}/dS, is determined by differentiating